Received: 4 May 2022 | Revised: 2 September 2022 | Accepted: 5 September 2022

DOI: 10.1002/ppp.2173

RESEARCH ARTICLE

WILEY

Spatial and temporal dynamics of *aufeis* in the Tso Moriri basin, eastern Ladakh, India

Dagmar Brombierstäudl[1] | Susanne Schmidt[1] | Marcus Nüsser[1,2]

[1]Department of Geography, South Asia Institute (SAI), Heidelberg University, Heidelberg, Germany

[2]Heidelberg Centre for the Environment (HCE), Heidelberg University, Heidelberg, Germany

Correspondence
Marcus Nüsser, Department of Geography, South Asia Institute (SAI), Heidelberg University, Heidelberg 69115, Germany.
Email: marcus.nuesser@uni-heidelberg.de

Funding information
Deutsche Forschungsgemeinschaft (DFG, German Research Foundation), Grant/Award Number: NU102/15-1

Abstract

Aufeis is a common phenomenon in cold regions of the Northern Hemisphere that develops during winter by successive water overflow and freezing on ice-covered surfaces. Most studies on *aufeis* occurrence focus on regions in North America and Siberia, while research in High Mountain Asia (HMA) is still in an exploratory phase. This study investigates the extent and dynamics of icing processes and *aufeis* in the Tso Moriri basin, eastern Ladakh, India. Based on a combination of 235 Landsat 5 TM/8 OLI and Sentinel-2 imagery from 2008 to 2021 the occurrence of icing and *aufeis* was classified using a random forest classifier. A total of 27 frequently occurring *aufeis* fields with an average maximum extent of 9 km^2 were identified, located at a mean elevation of 4,700 m a.s.l. Temporal patterns show a distinct accumulation phase (icing) between November and April, and a melting phase lasting from May until July. Icing is characterized by high seasonal and inter-annual variability. Successive water overflow mainly occurs between January and March and seems to be related to diurnal freeze–thaw-cycles, whereas higher daytime temperatures result in larger icing areas. *Aufeis* feeding sources are often located within or in close vicinity to wetland areas, while vegetation is largely absent on surfaces with frequent *aufeis* formation. These interactions require more attention in future research. In addition, this study shows the high potential of a machine learning approach to monitor icing processes and *aufeis*, which can be transferred to other regions.

KEYWORDS
icing, Landsat, remote sensing, time-series, Trans-Himalaya, water resource

1 | INTRODUCTION

Cryospheric changes have gained much attention as a major research topic in recent decades due to widespread consequences for biophysical and human systems alike. Climate change has already led to extensive glacier retreat and mass loss,[1–3] decrease in seasonal snow cover[4,5] and permafrost degradation.[6–10] In the snow-dominated and glacier-fed Himalayan basins, these changes affect the amount and seasonal patterns of run-off with impacts on irrigated agriculture[11,12] and hydropower generation.[13] However, the formation, extent and hydrological importance of river and lake ice have not been a major research topic, although these cryospheric components can be used as a proxy for regional climate change.[14–16] Only few studies have focused on river or lake ice phenology and monitoring in High Mountain Asia (HMA).[17–20] Closely related to these processes is the formation of *aufeis*,[21] which appears as seasonal, surficial bodies of

layered ice resulting from overflow of ground, spring or stream water onto frozen surfaces. Its complex formation is controlled by a combination of hydro-meteorological factors and permafrost distribution, but their interactions are poorly understood.[22,23] Unlike river ice, it persists throughout the spring melt season and larger *aufeis* fields – which may reach an average thickness of several metres over areas of several square kilometres in other northern high latitude regions, such as Alaska and Siberia[24] – can even persist over summer.[25] For several river systems in cold environments, *aufeis* volumes are estimated to store a substantial amount of winter discharge which becomes available in spring. Due to climate change, the number and extent of *aufeis* fields are declining in several cold regions.[23,25,26] Studies on *aufeis* have mainly been conducted in North America or Siberia,[27–30] while research in HMA is still in an exploratory phase, with only one inventory for the upper Indus basin (UIB).[31] This inventory comprises 3,700 *aufeis* fields, with most of them being located in the eastern parts of UIB, indicating that cold-arid conditions might be beneficial for their formation in high-altitude regions. Even though *aufeis* fields cover only a small proportion of the UIB (Figure 1), the physical process of *aufeis* accumulation has been used by local communities in Central Ladakh for the construction of ice reservoirs, which serve to cope with seasonal water scarcity in spring.[12,32–35]

The overall aim of this study is to explore the extent and dynamics of *aufeis* in the endorheic Tso Moriri basin of eastern Ladakh. Located in close proximity to the Tibetan plateau, it can be assumed that *aufeis* is a prominent landscape feature and of great importance for hydrological processes. According to Ensom et al.,[22] we distinguish between the process of accumulation (icing) and the resulting ice body (*aufeis*). For an improved understanding of the spatio-temporal distribution of icing processes and *aufeis* in this region, seasonal and inter-annual dynamics of icing and *aufeis* occurrence and depletion are analysed using a time-series approach based on Landsat and Sentinel-2 data.

2 | STUDY AREA

The endorheic Tso Moriri basin is part of the Changthang plateau located in Ladakh, northern India, and covers an area of 2,350 km^2 (Figure 2). Lake Tso Moriri (4,520 m a.s.l., 150 km^2 in size) is situated in the centre of the basin and is surrounded by the mountain ranges of Chamser to the east and Korzok to the west, which reach elevations above 6,650 m a.s.l. with small, high-altitude glaciers located above 5,400 m a.s.l.[36] More than 50% of the basin is snow covered in winter, which is reduced to less than 10% in summer.[37] The brackish lake is mainly fed by two perennial rivers and several rivulets which drain meltwater from snow and glaciers. Located in the rain shadow of the Greater Himalayan range, the basin receives only 100–300 mm annual precipitation. Mean monthly temperatures range from around −20°C in January to around 8°C in July, with an annual mean of about −2°C.[38–41]

Due to the cold-arid climate, densely vegetated wetlands are restricted to moist alluvial and slightly saline soils, which are rich in organic material and sharply contrast to the surrounding sparsely

FIGURE 1 *Aufeis* fields in different locations of Ladakh [Colour figure can be viewed at wileyonlinelibrary.com]

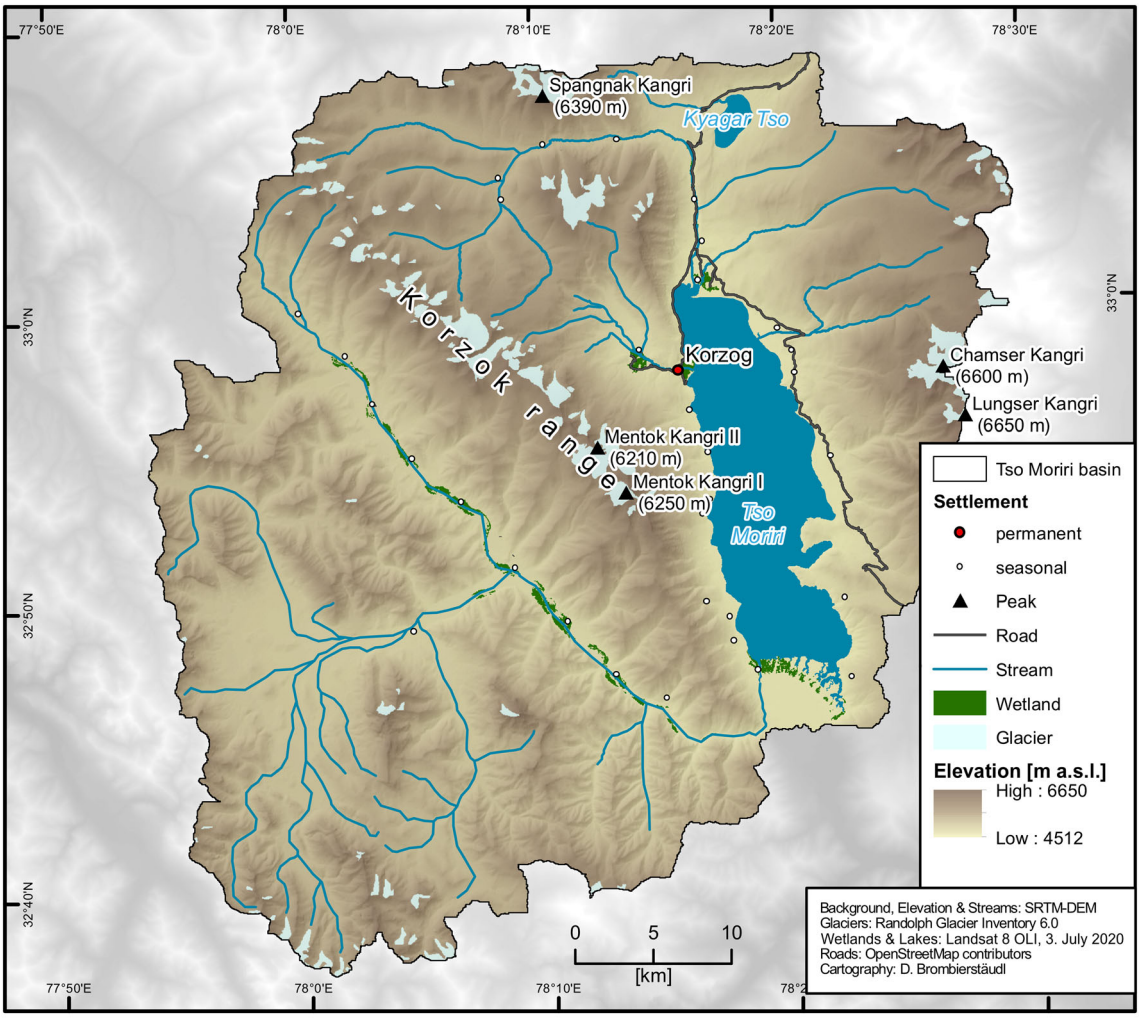

View from Chamser Kangri (M. Nüsser, 02. September 2013)

FIGURE 2 The Tso Moriri basin, eastern Ladakh, Trans-Himalaya [Colour figure can be viewed at wileyonlinelibrary.com]

vegetated slopes. Dominant plants of the wetlands include *Kobresia schoenoides* (C.A. Mey.) Steud., *Kobresia royleana* (Nees) Boeck., *Blysmus compressus* (L.) Panzer ex Link, *Poa calliopsis* Litw. ex Ovcz. and *Puccinellia himalaica* Tzvelev. Surrounding desert steppe plant communities on the hillslopes include *Krascheninnikovia ceratoides* (L.) Gueldenst., *Stipa caucasica* Schmalh., *Stipa subsessiliflora* (Rupr.) Roshev.; and specifically on sand flats: *Carex moorcroftii* Falc. ex. Boott, *Leymus secalinus* (Georgi) Tzvelev and *Oxytropis tatarica* Cambess. ex Bunge (own plant sampling in 2017, unpublished).

Pastoralism has historically been the main source of livelihood under these harsh environmental conditions. Wetlands around the lakes and along the streams are used as pastures for domestic sheep, goats, yaks and horses.[42] Several seasonal grazing settlements exist along the lake and rivers, inhabited between May and October. The only permanent settlement is Korzok (Korzog) with a small area under cultivation located at the western shore of Tso Moriri, which serves as a regional economic and tourism centre. Due to the high ecological diversity and its importance as a breeding area for several bird

species,[43,44] Tso Moriri was designated as a wetland of international importance under the Ramsar convention in 2002.[45]

3 | MATERIALS AND METHODS

3.1 | Materials

Data from Landsat and Sentinel-2 missions from November to July were utilized to map icing patterns and *aufeis* fields. The start of the time-series analysis was set to 2008, because data availability in the region is sparse was previous years, mainly due to a non-operational ground station in South and Central Asia.[46–48] Landsat Collection 2 Level 2 surface reflectance imagery (paths/row: 146–147/036) was selected because of its improved geolocation accuracy and interoperability with Sentinel-2 data. Since 2018, imagery from both Sentinel-2 satellites was continuously available (Tile: T44SKB). Level-1C product (top-of-atmosphere) was used due to artefacts and oversaturation in some scenes of Level-2 surface reflectance product. The combination of Landsat and Sentinel-2 data results in a varying number of images per year and month, with the largest number for the years 2018–2021. No images are available between November 2011 and February 2013, the period between the decommission of Landsat 5 TM and the start of Landsat 8 Operational Land Imager (OLI) mission. Both data sets were acquired from the USGS EarthExplorer (https://earthexplorer.usgs.gov). In total, 235 images with cloud-free main valleys were analysed, of which 171 were allotted to Landsat and the remaining 64 to Sentinel-2 (Figure 3; Table S1).

The extent of the Tso Moriri watershed, slope and elevation values were derived from the 1 Arc-Second Global SRTM-DEM (Shuttle Radar Topography Mission-Digital Elevation Model) with a spatial resolution of 30 m downloaded from https://earthexplorer.usgs.gov/.

The Moderate Resolution Imaging Spectroradiometer (MODIS) daily land surface temperature (LST) data set from the Terra (MOD11A1 V6) and Aqua (MYD11A1 V6) satellites with a spatial resolution of 1 km was used to substitute non-available in-situ climate data and to estimate surface temperatures. LST obtained using MODIS represents the radiometric temperature of a given surface and is not the same as standard air temperature measured 2 m above the ground.[49] Depending on land cover and atmospheric conditions LST_{day} can be up to 20°C higher than air temperature.[50,51] MODIS LST are considered a valuable data set for studies of land surface processes, as the evaluations of LST_{day} to in-situ surface temperature measurements have shown good agreements.[52–55] Each satellite provides two acquisitions, one daytime and one night-time observation. Local crossing times were ~10:30 am/ ~10:30 pm for Terra and ~1:30 am / ~1:30 pm for Aqua. The Aqua daytime acquisition was chosen for subsequent analysis as it best represents the maximum temperature of the land surface (LST_{day}). In addition, Aqua night-time data (LST_{night}) were used to show the seasonality of freeze–thaw cycles (see Suppl. S2).

3.2 | Pre-processing

For all Landsat and Sentinel-2 images the normalized difference snow index (NDSI)[56]:

$$NDSI = \frac{\text{Green} - \text{SWIR1}}{\text{Green} + \text{SWIR1}} \quad (1)$$

was calculated and stacked into a multi-band raster image containing seven bands (blue, green, red, near-infrared (NIR), shortwave infrared 1 (SWIR 1), shortwave infrared 2 (SWIR 2), NDSI). For Sentinel-2, the visible (blue, green, red) and NIR bands were resampled to 20 m to

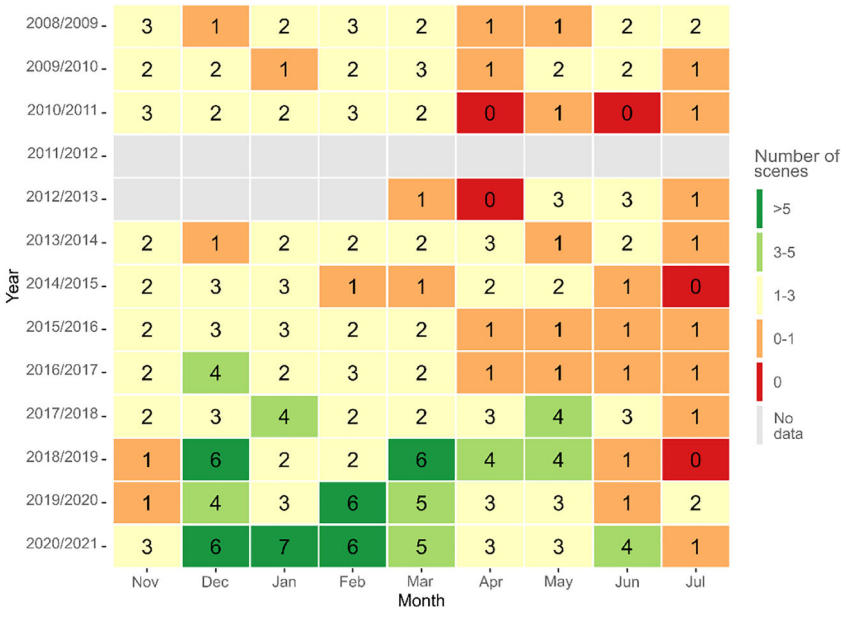

FIGURE 3 Number of used Landsat and Sentinel-2 scenes per year and month. 0 is caused by high cloud coverage, no data due to the transition period between the decommission of Landsat 5 TM and the start of Landsat 8 OLI [Colour figure can be viewed at wileyonlinelibrary.com]

match the spatial resolution of SWIR bands. All steps were conducted with Python 3.7.6 and R, version 4.1.0.[57]

MODIS LST data were processed using the cloud-based Google Earth Engine (GEE) computing platform.[58] Temperature was extracted on six data points along the river courses of the main valleys and separately averaged for daytime (1:30 pm) and for night-time (1:30 am) data. To obtain a consistent timeline and to reduce biasness associated with missing values, LST_{day} and LST_{night} were aggregated each into 8-day averages, if fewer than three observations within the respective 8-day period contained no data. Otherwise the time frame was excluded (Figure S2). Based on this 8-day period, an 11-year average of LST_{day} was calculated as a baseline for yearly absolute temperature anomalies, which were used to explore their influence during *aufeis* accumulation.

3.3 | Mapping of icing events and *aufeis*

Icing and *aufeis* show a consistent lower albedo in the VIS/NIR parts of the electromagnetic spectrum compared to snow (Figure 4). Thus, icing events appear in a turquoise colour, while snow remains white in a NIR-R-G false colour composite.

Although this distinct spectral signature of icing and *aufeis* enables its detection with normalized difference snow index (NDSI)-based threshold techniques,[23,26,31] their application to image time-series often requires time-intensive manual adaptation of thresholds for each scene. Therefore, the delineation of icing and *aufeis* was performed using a random forest (RF) classifier (R *randomForest* package[59]). RF is a non-parametric supervised machine learning algorithm and has been frequently applied in various remote sensing studies, e.g., mapping of global lake ice cover,[60] supraglacial lakes[61,62] or wetland inventorying.[63] An RF draws predictions from an ensemble of uncorrelated Classification and Regression Trees (CART) which are built on the basis of randomly selected subsets of training samples. Two-thirds of the training samples are used to train the trees, while the remaining one-third is used for an internal cross-validation of model performance. Each decision tree is produced independently, and each node is split by a user-defined number of features (*mtry*). The forest is then grown up to a user-defined number of trees (*ntree*). For new data, each class is predicted based on majority votes of all decision trees.[64] Compared to other machine learning algorithms, RF is less prone to overfitting, has parallel processing capabilities and only requires the setting of a few parameters[65,66]

After evaluation of several combinations, five bands were selected as predictor bands: green, red, NIR, SWIR 1 and NDSI. The RF was built using a *mtry* value of 2 and the default *ntree* value of 500.

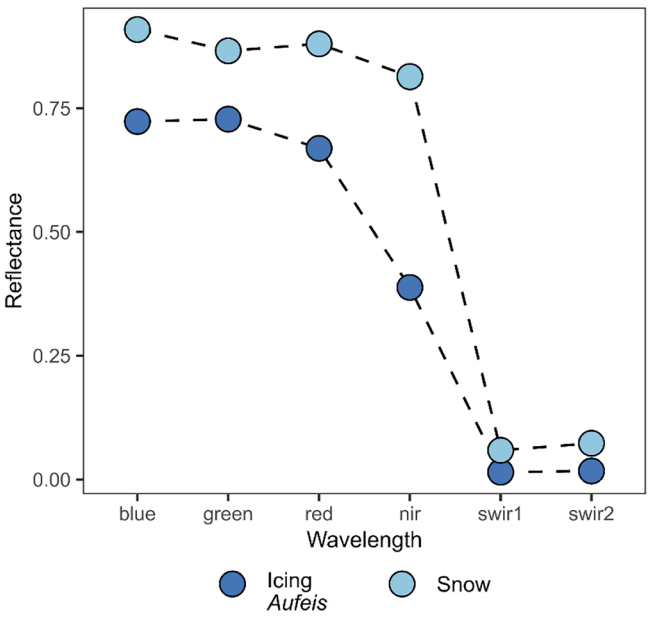

FIGURE 4 Averaged spectral curves from Landsat imagery for icing and *aufeis* (dark blue) and seasonal snow cover (light blue) in the visible to shortwave infrared [Colour figure can be viewed at wileyonlinelibrary.com]

3.4 | Training and validation samples

Two RFs were trained, one for Landsat and one for Sentinel-2 imagery using the same settings and predictor bands. For training and validation two separate data sets were created manually on false-colour composites due to the lack of adequate field data. For the delineation of training pixels, 15 Landsat and 10 Sentinel-2 scenes were randomly selected to cover a wide range of spectral properties throughout the whole observation period. To minimize spectral confusion, four land cover classes (Icing/*aufeis*, snow, barren land, topographic shadows) were distinguished (Table S2). For each pixel, the spectral values on the specific date were extracted for the predictor bands.

Training samples were selected following an area-proportional approach with sample allocation according to the expected area of each class.[67] Therefore, 25% of icing/*aufeis* and 60% of samples for each of the remaining classes were chosen randomly, and the remaining pixels discarded. Validation data sets contain 200–300 samples for each classification.

3.5 | Post-classification

To create binary classifications, the classes snow, barren land and topographic shadow were merged into one non-*aufeis* class. Slopes ≥10° were excluded with a slope mask derived from the SRTM-DEM as icing and *aufeis* in the neighbouring UIB mainly occurs on slopes with angles of <10°.[31] Finally, a majority filter was applied to eliminate pixel clusters smaller than four Landsat pixels (3,600m^2).[22] This refined classification was the basis for the accuracy assessment, which reached a very good agreement with an overall average Kappa coefficient of 0.86. Details on this procedure are provided in the supplement (Text S1; Figure S1). Remaining misclassifications were manually

removed after the accuracy assessment (Figure 5). Classification results were categorized into icing (accumulation: November–April) and *aufeis* (melting: May–July).

As spring is the optimal time to detect the maximum possible number and size of *aufeis* fields,[23,26] scenes closest to mid-May were chosen to calculate the average area and the return frequency of individual *aufeis* fields (Table S3).

To determine areas subject to icing occurrence and the return frequency of *aufeis*, the count of instances when ice was present at a pixel was calculated. The return frequency was divided into three classes following a categorization by Morse & Wolfe[23] as either infrequent (<3 years), occasional (≥3 and < 6 years) or frequent (≥6 years).

4 | RESULTS

4.1 | *Aufeis* in the Tso Moriri basin

Frequently occurring (≥6 out of 11 years analysed) *aufeis* ranging from 0.007 km^2 up to 1.7 km^2 in size are predominately located along the two main valleys: 22 are found along the southern river and its tributary streams, whereas only 4 are detected along the northern valleys and only 1 on the fluvial fan of Korzog. The mean *aufeis*-covered area in the study period amounts to a maximum of 9 km^2 in May over the entire observation period. *Aufeis* larger than 0.5 km^2 are found only along the southern inlet. The elevational distribution of individual *aufeis* fields follows the topography of the basin and decreases from 5,040 to 4,520 m a.s.l. from northwest to southeast towards the lake (Figure 6).

4.2 | Icing process: Temporal accumulation and melting patterns

Temporal dynamics reveal highly variable seasonal and inter-annual patterns. However, two main phases can be distinguished: the icing and melting phases, which are mainly temperature controlled. The annual icing process starts in November with a drastic growth in December (Figure 7) and lasts until April, when day- and night-time temperature differences are highest (Figure S2). This phase is characterized by regular water overflow and freezing onto the

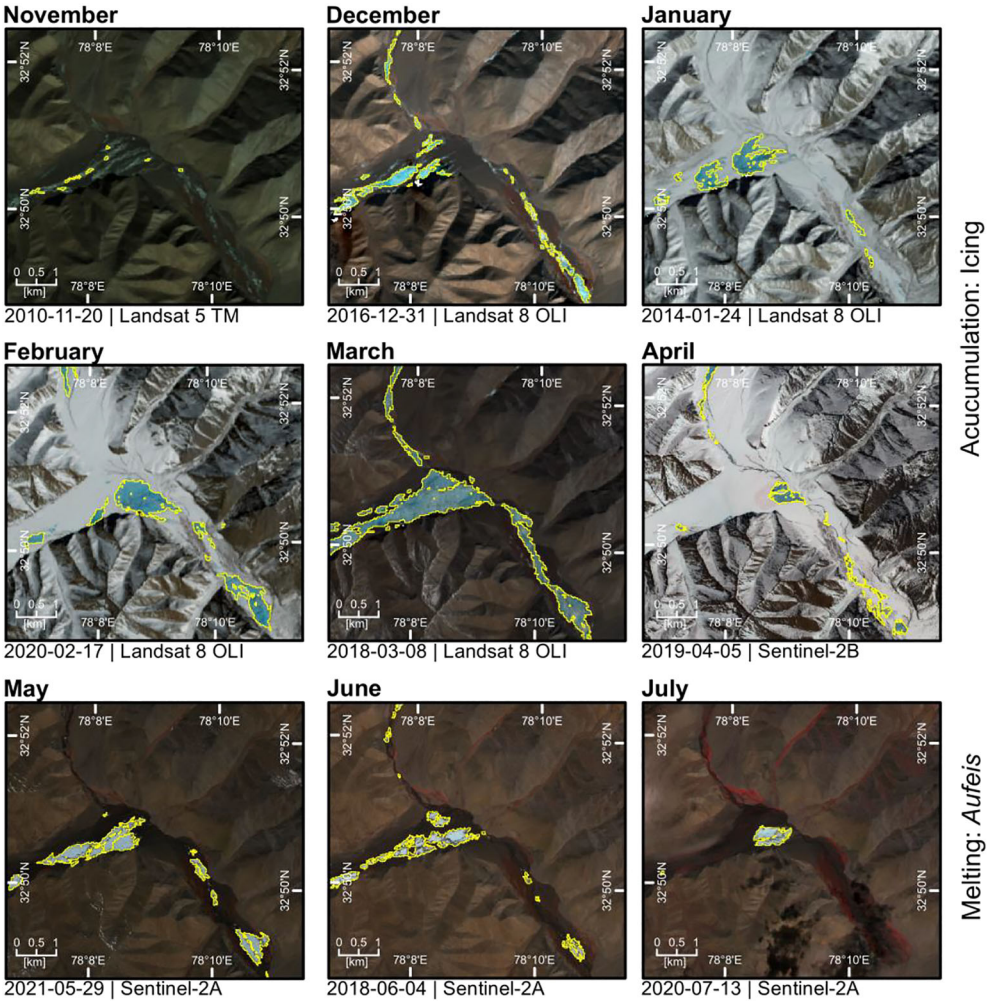

FIGURE 5 Exemplary classification results after post-processing for different months, years and sensors. Icing and *aufeis* extents (yellow) are shown on false-colour composites (NIR-R-G) [Colour figure can be viewed at wileyonlinelibrary.com]

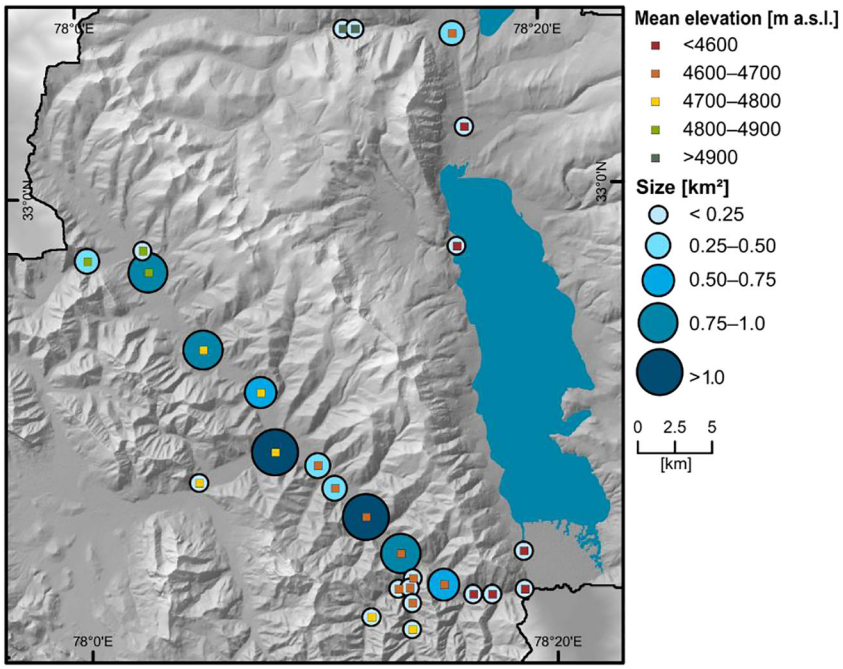

FIGURE 6 Spatial distribution, size and mean elevation of *aufeis* in the Tso Moriri basin [Colour figure can be viewed at wileyonlinelibrary.com]

surface. Icing occurrence is most prominent from January through March and displays a strong relation to the degree of snow coverage and LST_{day} anomalies compared to the 11-year average. This pattern is especially evident in 2018, which displays constantly high temperature anomalies together with largest icing areas (~16 km^2). In contrast, below 11-year average temperatures, i.e., from January to March for 2015, 2017 and 2019, favour longer snow coverage, which results in smaller visible icing areas (between 4 and 8 km^2). This pattern is also expressed in moderate to strong correlation ($R = 0.64$) with a very high statistical significance ($p < 0.0001$) (Figure 8).

Months with a moderate snow coverage show alternating seasonal and inter-annual patterns in icing area, depending on the location of snow within the valleys. It shows no relation to the amount of icing occurring in the previous months. Melting of *aufeis* is detectable from May onwards, and its area continually decreases until the end of July (Figure 7).

4.3 | Icing and *aufeis* accumulation frequency

Spatial icing expansion along the southern inlet of Tso Moriri can be differentiated into two forms. While separate icing areas are present in the upstream parts of the river (Figure 9a,b), icing in the downstream sections merges into one large ice field (Figure 9c,d). Both types are not restricted to the river channels, but rather cover the entire floodplains. Icing zones are spatially and inter-annually consistent throughout the watershed with the exception of the large alluvial fan to the south of the lake (Figure 9c). In general, icing occurrence is highest in the centre and gradually reduces with distance and lateral expansion from the source. Potential discharge points for water overflow are often located within or close to wetland areas. In total, 20% of the main valleys are subject to icing occurrence.

Aufeis frequency corresponds with vegetation distribution on the floodplain. Dense vegetation is found only in areas with low return frequencies (infrequent/occasional) and is almost absent in areas where ice returns on a frequent basis (Figure 9A–D). Wetland areas are not subject to *aufeis* development, but are found in close proximity along the edges of frequently returning *aufeis*.

However, icing does not necessarily lead to frequent *aufeis* accumulation, e.g., as seen on the west side of the alluvial fan. In general, four categories regarding the connection between icing and accumulation can be differentiated in the basin: (i) Frequent overflow but no *aufeis* accumulation, (ii) frequent overflow with *aufeis* accumulation, (iii) infrequent to occasional overflow events but *aufeis* accumulation and (iv) infrequent to occasional overflow events resulting in no *aufeis*.

Considering the extent in May, the area decreases with increasing return frequency and is lowest for pixels ice-covered every year. Infrequent *aufeis*-covered pixels have the largest share compared to the remaining classes with 12.55 km^2 and are mainly located around the edges. *Aufeis* occurring on a frequent basis (9 km^2) is 3.15 km^2 larger compared to only occasional appearing ice (5.93 km^2).

5 | DISCUSSION

In general, the pattern of *aufeis* development resembles river ice phenology,[68] even though it does not disappear rapidly during spring but rather gradually decreases between May and July. Melt of individual *aufeis* is spatially and temporally heterogeneous with great annual variability. It seems not to be only influenced by temperature, but also

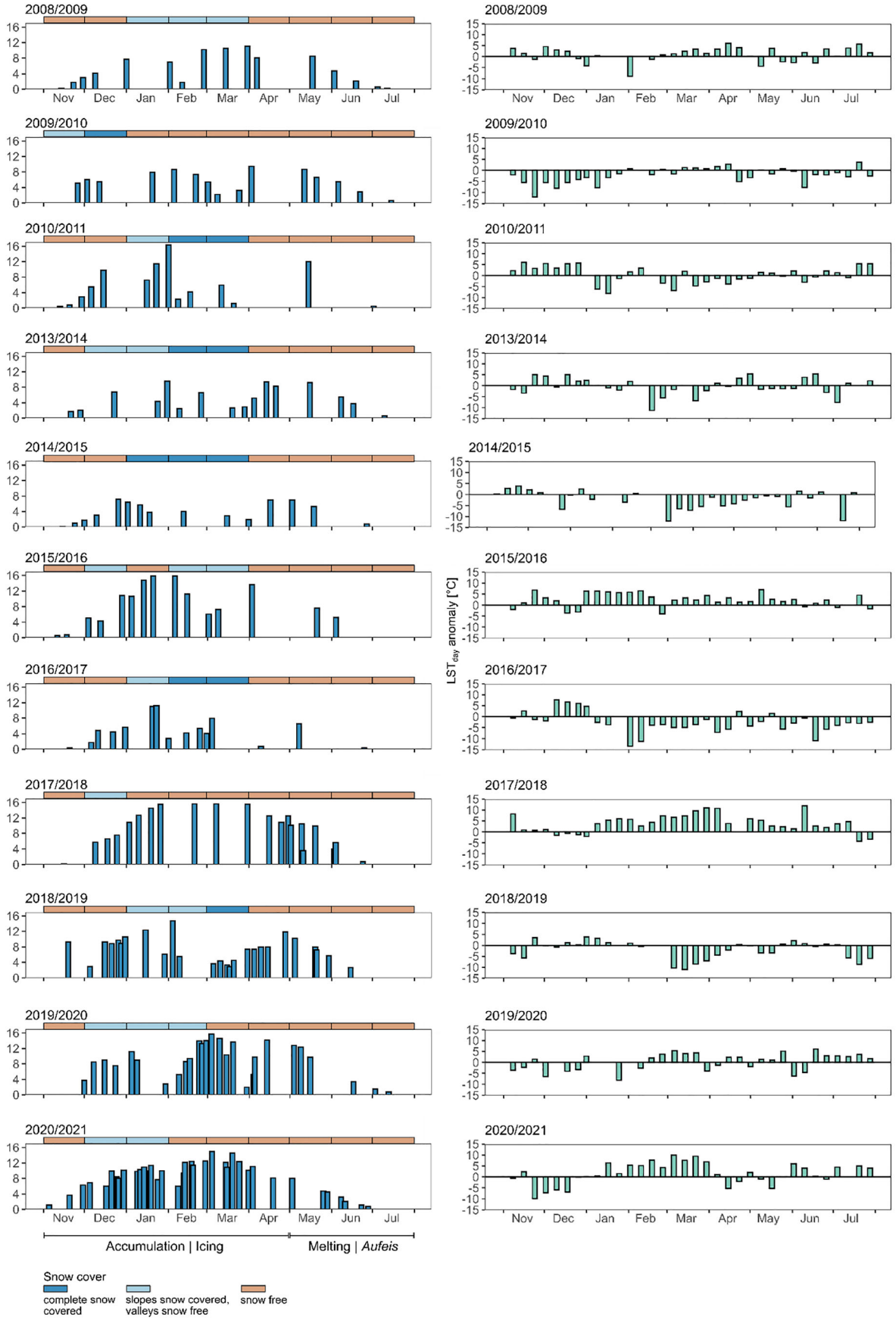

FIGURE 7 Icing/*aufeis* area (left), observed snow coverage for each observation of the time-series (2008/2009–2020/2021) and LST_{day} anomalies (right). 2011/2012 & 2012/2013 were excluded due to data gaps [Colour figure can be viewed at wileyonlinelibrary.com]

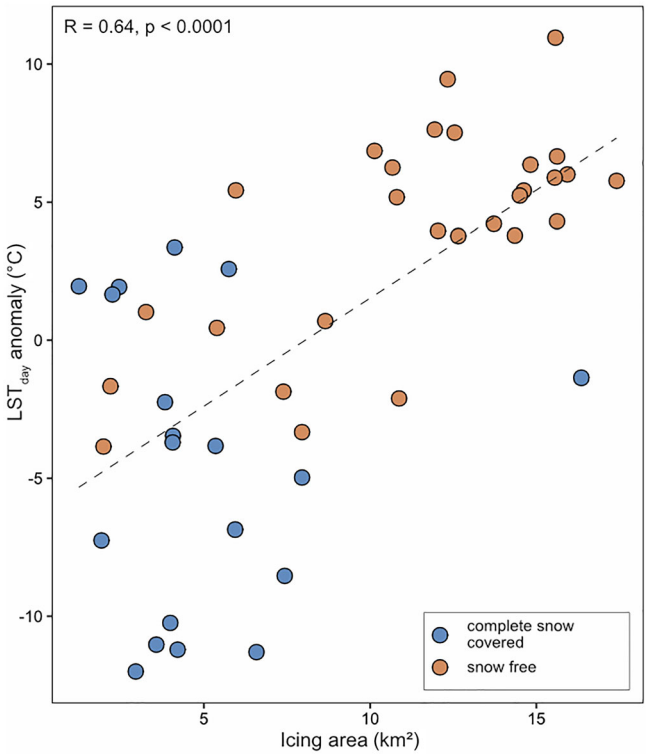

FIGURE 8 Scatterplot of LST_{day} anomaly and icing area in the most important months for accumulation (January–March) according to snow coverage. A moderate to strong correlation ($R = 0.64$) with a very high statistical significance ($p < 0.0001$) is detectable [Colour figure can be viewed at wileyonlinelibrary.com]

probably by a combination of factors, including ice thickness, cloud coverage and solar radiation.[69] LST_{day} anomalies indicate an inverse relationship where above-average temperatures are beneficial for water overflow events, while at the same time low temperatures at night facilitate the freezing process. This is particularly visible from January to March, which can be considered the most important months for the formation of *aufeis* fields. Although April is still characterized by a high degree of water overflow, surface temperatures might already be too high for frequent icing events and can be regarded as a transitional month, where diurnal melting has already started or freezing overnight is still occurring. Despite not utilizing air temperature as a meteorological variable, the results still suggest the occurrence of warming intervals, which might be one of the key factors in determining at what time an overflow event happens. While statistical analysis has indicated the importance of short-term air temperature increases for overflow events,[23,30] the impact of LST on overflow remains unknown yet. Therefore, it might be valuable to include LST data in future studies to obtain a better understanding of *aufeis* accumulation.

Icing dynamics are further affected by snow cover thickness and duration, where higher daytime air temperatures cause a shorter duration or complete melting of snow cover along the valleys and lead to greater icing sizes. This inverse relationship between snow cover and extent of icing has also been suggested in other studies.[21,27] Despite that, the spatial extent of icing does not determine the final size of *aufeis* fields, which show rather stable extents irrespective of the amount of water overflows during accumulation. Although the applied remote sensing approach does not allow for quantification of ice thickness, this parameter could either be estimated by field measurements or the application of terrestrial or satellite-based photogrammetry techniques, it can be assumed that ice thickness of individual *aufeis* fields varies on an inter-annual basis.

The high-altitude wetlands are not only of great environmental importance but also serve as important grazing grounds. They are primarily sustained by snow and glacier meltwater[70] and permafrost[71] meltwater. The close proximity of *aufeis* fields to wetlands suggests that they supply additional water to those ecosystems, especially during melting at the onset of the vegetation period between May and June and in turn their substantial contribution for groundwater recharge in cold-arid high mountain regions.[72] In addition, potential water sources feeding the *aufeis* are often located close or within wetlands indicating their importance for *aufeis* development. Thus, climate change will most likely affect icing and *aufeis* dynamics in HMA, but it is not applicable to make assumptions about possible trends based on this study as the observation period only represents 11 years. Such developments have already been observed in other *aufeis*-affected regions, where the number, extent and persistence are already declining.[23,25,26,73] Nevertheless, remote sensing provides the opportunity to monitor such changes, despite data availability remaining the main obstacle for long-term monitoring in the region. The widespread occurrence of *aufeis* in the Trans-Himalaya[31] offers the opportunity not only to investigate the hydrology or physicomechanical process but also their role for river ecology, downstream habitats or local communities – aspects which have not received much attention so far.[28]

The results of the accuracy assessment support that a machine learning approach is suitable to map icing/*aufeis* and that the method can be transferred to other regions. Unlike thresholds, deviations in spectral properties do not require manual adjustments and have little influence on the predictions of the model, if the training samples are representative of the target classes.[65] This drastically reduces the workload especially in cases where large amounts of data are analysed. In addition, the combination of Landsat and Sentinel-2 imagery offers the possibility to analyse denser time-series at a medium and high spatial resolution which provides more detailed insights into icing dynamics. However, the lower temporal resolution also has disadvantages in the detection of icing areas. Smaller detectable areas may be caused by snowfall events prior to the satellites acquisition. Data from sensors with a higher temporal resolution, like MODIS daily surface reflectance imagery, can be an adequate alternative to map intra- and inter-annual variations in icing/*aufeis*,[25] but this comes with the disadvantage of a low spatial resolution. To mitigate the problem of cloud coverage, synthetic aperture radar (SAR) has already been successfully used to map icing and *aufeis*.[24,30,74] However, the application of SAR data can be challenging in areas with rugged topography due to distortion caused by the complex image geometry.

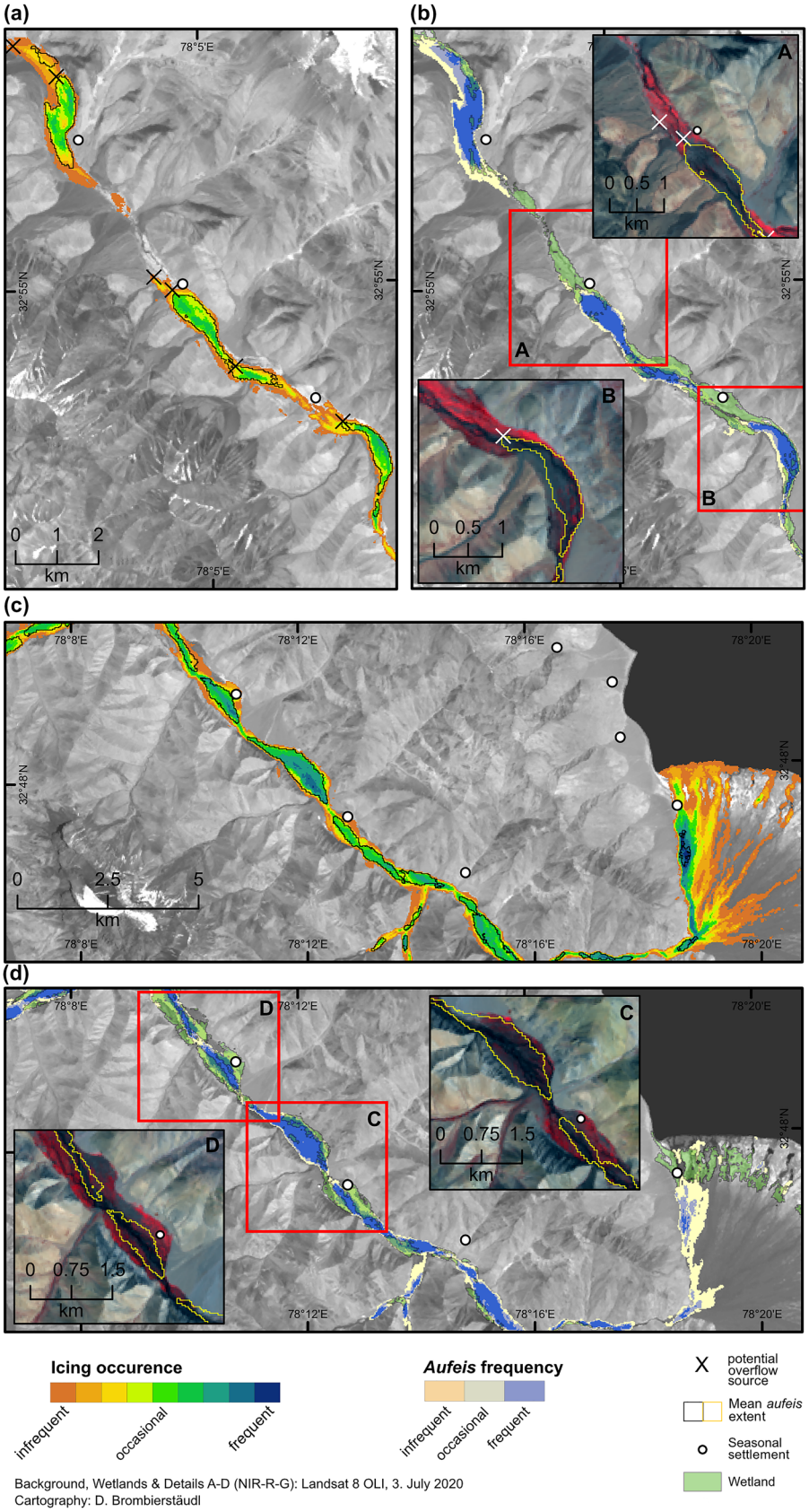

FIGURE 9 Icing occurrence (a and c) and *aufeis* frequency (b and d). A–D shows the vegetation extent in comparison to *aufeis* frequency. The thin black (a–d) and yellow (A–D) lines refer to the mean *aufeis* extent. Icing occurrence and *aufeis* frequency were calculated based on the count of instances when ice was present at a pixel. Categorization was adapted from Morse & Wolf[23] [Colour figure can be viewed at wileyonlinelibrary.com]

6 | CONCLUSION

In this study, icing patterns and *aufeis* occurrence in the Tso Moriri basin were mapped using a time-series approach of freely available Landsat and Sentinel-2 data. A total of 27 *aufeis* fields covering an average area of 9 km^2 were identified. Although icing occurrence is highly variable on the seasonal and inter-annual scale, resulting *aufeis* bodies form at the same place year after year. In addition, their location in close proximity to the high-altitude wetlands suggests close hydrological interactions and dependencies. This emphasizes the need to pay particular attention to the function of *aufeis* in the ecological system. In addition, the machine learning approach of this study provides a new opportunity for almost completely automated mapping of icing and *aufeis*. This method can be particularly useful for studies utilizing a large amount of satellite data as adaptation of thresholds for individual scenes is not required. However, it does not permit conclusions about *aufeis* thickness or volume. Therefore, future research should integrate additional methods, e.g., photogrammetric techniques, to estimate these parameters to contribute to a better understanding of *aufeis* and its role in HMA.

ACKNOWLEDGEMENTS

Research for the project is funded by the German Research Foundation (Deutsche Forschungsgemeinschaft, DFG) in the context of the project 'Exploring Aufeis: Relevance of Icing and Ice Reservoirs for Climate Change Adaptation in the Trans-Himalaya of Ladakh, India' (NU102/15-1). The study was first presented on the Alpine Glaciology Meeting 2022 in Munich and the ESA Living Planet Symposium 2022 in Bonn. The authors are thankful to the USGS and ESA for providing Landsat, MODIS and Sentinel imagery. The authors also thank Mauro Guglielmin, Nicolas Jelinski and two anonymous reviewers for their valuable comments which helped to improve the manuscript. Open Access funding enabled and organized by Projekt DEAL.

DATA AVAILABILITY STATEMENT

The data that support the findings of this study are available from the corresponding author upon reasonable request.

ORCID

Dagmar Brombierstäudl https://orcid.org/0000-0001-5704-0634
Susanne Schmidt https://orcid.org/0000-0002-6200-4539
Marcus Nüsser https://orcid.org/0000-0002-8626-8336

REFERENCES

1. Armstrong RL, Rittger K, Brodzik MJ, et al. Runoff from glacier ice and seasonal snow in high Asia: separating melt water sources in river flow. *Regional Environmental Change*. 2019;19(5):1249-1261. doi:10.1007/s10113-018-1429-0
2. Farinotti D, Huss M, Fürst JJ, et al. A consensus estimate for the ice thickness distribution of all glaciers on earth. *Nat Geosci*. 2019;12(3):168-173. doi:10.1038/s41561-019-0300-3
3. Zemp M, Huss M, Thibert E, et al. Global glacier mass changes and their contributions to sea-level rise from 1961 to 2016. *Nat*. 2019;568(7752):382-386. doi:10.1038/s41586-019-1071-0
4. Bolch T, Shea JM, Liu S, et al. Status and change of the cryosphere in the extended Hindu Kush Himalaya region. In: Wester P, Mishra A, Mukherji A, Shrestha AB, eds. *The Hindu Kush Himalaya assessment: Mountains, climate change, sustainability and people*. Springer; 2019:209-255.
5. Dharpure JK, Goswami A, Patel A, Kulkarni AV, Snehmani. Assessment of snow cover variability and its sensitivity to hydrometeorological factors in the Karakoram and Himalayan region. *Hydrol Sci J*. 2021;66(15):2198-2215. doi:10.1080/02626667.2021.1985125
6. Biskaborn BK, Smith SL, Noetzli J, et al. Permafrost is warming at a global scale. *Nat Commun*. 2019;10(1):264 doi:10.1038/s41467-018-08240-4
7. Gao T, Zhang T, Cao L, Kang S, Sillanpää M. Reduced winter runoff in a mountainous permafrost region in the northern Tibetan plateau. *Cold Reg Sci Technol*. 2016;126:36-43. doi:10.1016/j.coldregions.2016.03.007
8. Hock R, Rasul G, Adler C, et al. High Mountain Areas. In: Pörtner H-O, Roberts DC, Masson-Delmotte V, et al., eds. *IPCC special report on the ocean and cryosphere in a changing climate*. Cambridge University Press; 2019:131-202. doi:10.1017/9781009157964.004.
9. IPCC. Climate Change 2013: The Physical Science Basis. In: Stocker TF, Qin D, Plattner G-K, et al., eds. *Contribution of working group I to the fifth assessment report of the intergovernmental panel on climate change*. Cambridge University Press; 2013. doi:10.1017/CBO9781107415324
10. IPCC. Climate Change 2021: The Physical Science Basis. In: Masson-Delmotte V, Zhai P, Pirani A, et al., eds. *Contribution of working group I to the sixth assessment report of the intergovernmental panel on climate change*. Cambridge University Press; 2021: in press. doi:10.1017/9781009157896.
11. Immerzeel WW, Van Beek LPH, Bierkens MFP. Climate change will affect the Asian water towers. *Science*. 2010;328(5984):1382-1385. doi:10.1126/science.1183188
12. Nüsser M, Dame J, Kraus B, Baghel R, Schmidt S. Socio-hydrology of "artificial glaciers" in Ladakh, India: assessing adaptive strategies in a changing cryosphere. *Regional Environmental Change*. 2019;19(5):1327-1337. doi:10.1007/s10113-018-1372-0
13. Nie Y, Pritchard HD, Liu Q, et al. Glacial change and hydrological implications in the Himalaya and Karakoram. *Nature Reviews Earth & Environment*. 2021;2:91-106. doi:10.1038/s43017-020-00124-w
14. Latifovic R, Pouliot D. Analysis of climate change impacts on lake ice phenology in Canada using the historical satellite data record. *Remote Sens Environ*. 2007;106(4):492-507. doi:10.1016/J.RSE.2006.09.015
15. Mishra V, Cherkauer KA, Bowling LC, Huber M. Lake ice phenology of small lakes: impacts of climate variability in the Great Lakes region. *Global Planet Change*. 2011;76(3–4):166-185. doi:10.1016/J.GLOPLACHA.2011.01.004
16. Newton AMW, Mullan DJ. Climate change and northern hemisphere lake and river ice phenology from 1931–2005. *The Cryosphere*. 2021;15(5):2211-2234. doi:10.5194/tc-15-2211-2021
17. Cai Y, Ke C-Q, Li X, Zhang G, Duan Z, Lee H. Variations of Lake ice phenology on the Tibetan plateau from 2001 to 2017 based on MODIS data. *Journal of Geophysical Research-Atmospheres*. 2019;124(2):825-843. doi:10.1029/2018JD028993
18. Kropáček J, Maussion F, Chen F, Hoerz S, Hochschild V. Analysis of ice phenology of lakes on the Tibetan plateau from MODIS data. *The Cryosphere*. 2013;7(1):287-301. doi:10.5194/tc-7-287-2013
19. Li H, Li H, Wang J, Hao X. Monitoring high-altitude river ice distribution at the basin scale in the northeastern Tibetan plateau from a Landsat time-series spanning 1999–2018. *Remote Sens Environ*. 2020;247:111915. doi:10.1016/j.rse.2020.111915
20. Li H, Li H, Wang J, Hao X. Identifying river ice on the Tibetan plateau based on the relative difference in spectral bands. *J Hydrol*. 2021;601:126613. doi:10.1016/j.jhydrol.2021.126613

21. Carey KL. Icings developed from surface water and ground water. *US Army Cold Regions Research and Engineering Laboratory Monograph III-D3*. 1973;67.
22. Ensom T, Makarieva O, Morse P, Kane D, Alekseev V, Marsh P. The distribution and dynamics of aufeis in permafrost regions. *Permafrost and Periglacial Processes*. 2020;31(3):383-395. doi:10.1002/ppp.2051
23. Morse PD, Wolfe SA. Geological and meteorological controls on icing (aufeis) dynamics (1985 to 2014) in subarctic Canada. *J Geophys Res Earth Surf*. 2015;120(9):1670-1686. doi:10.1002/2015JF003534
24. Shusan L, Benson C, Shapiro L, Dean K. Aufeis in the Ivishak River, Alaska, mapped from satellite radar interferometry. *Remote Sens Environ*. 1997;60(2):131-139. doi:10.1016/S0034-4257(96)00167-8
25. Pavelsky TM, Zarnetske JP. Rapid decline in river icings detected in Arctic Alaska: implications for a changing hydrologic cycle and river ecosystems. *Geophys Res Lett*. 2017;44(7):3228-3235. doi:10.1002/2016GL072397
26. Makarieva O, Shikhov A, Nesterova N, Ostashov A. Historical and recent aufeis in the Indigirka River basin (Russia). *Earth System Science Data*. 2019;11(1):409-420. doi:10.5194/essd-11-409-2019
27. Harden D, Barnes P, Reimnitz E. Distribution and character of Naleds in northeastern Alaska. ARCTIC. 1977;30(1):1-30. doi:10.14430/arctic2681
28. Huryn AD, Gooseff MN, Hendrickson PJ, Briggs MA, Tape KD, Terry NC. Aufeis fields as novel groundwater-dependent ecosystems in the arctic cryosphere. *Limnol Oceanogr*. 2021;66(3):607-624. doi:10.1002/lno.11626
29. Osokin IM. Regime of naleds in trans-Baikal region. In: *Second international conference on permafrost*. National Research Council; 1973:391-396.
30. Yoshikawa K, Hinzman LD, Kane DL. Spring and aufeis (icing) hydrology in Brooks Range, Alaska. *J Geophys Res Biogeo*. 2007;112(G4):1-14. doi:10.1029/2006JG000294
31. Brombierstäudl D, Schmidt S, Nüsser M. Distribution and relevance of *aufeis* (icing) in the upper Indus Basin. *Sci Total Environ*. 2021;780:146604. doi:10.1016/j.scitotenv.2021.146604
32. Clouse C, Anderson N, Shippling T. Ladakh's artificial glaciers: climate-adaptive design for water scarcity. *Clim Dev*. 2017;9(5):428-438. doi:10.1080/17565529.2016.1167664
33. Dar SR, Norphel C, Akhoon MM, et al. Man's artificial glacier—a way forward toward water harvesting for pre and post sowing irrigation to facilitate early sowing of wheat in cold arid Himalayan deserts of Ladakh. *Renewable Agriculture and Food Systems*. Published online November. 2017:1-10. doi:10.1017/S1742170517000527
34. Norphel C, Tashi P. Snow Water Harvesting in the Cold Desert in Ladakh: An Introduction to Artificial Glaciers. In: Nibanupudi H, Shaw R, eds. *Mountain hazards and disaster risk reduction*. Tokyo: Springer; 2015:199-210. doi:10.1007/978-4-431-55242-0_11.
35. Nüsser M, Baghel R. Local Knowledge and Global Concerns: Artificial Glaciers as a Focus of Environmental Knowledge and Development Interventions. In: Meusburger P, Freytag T, Suarsana L, eds. *Ethnic and cultural dimensions of knowledge*. Knowledge and Space, vol. 8. Cham: Springer; 2016:191-209. doi:10.1007/978-3-319-21900-4_9.
36. Schmidt S, Nüsser M. Changes of high altitude glaciers in the trans-Himalaya of Ladakh over the past five decades (1969–2016). *Geosciences*. 2017;7(2):27. doi:10.3390/geosciences7020027
37. Passang S, Schmidt S, Nüsser M. Topographical impact on snow cover distribution in the trans-Himalayan region of Ladakh, India. *Geosciences*. 2022;12(8):311. doi:10.3390/geosciences12080311
38. Dolezal J, Dvorsky M, Kopecky M, et al. Vegetation dynamics at the upper elevational limit of vascular plants in Himalaya. *Sci Rep*. 2016;6:24881. doi:10.1038/srep24881
39. Dvorský M, Chlumská Z, Altman J, et al. Gardening in the zone of death: an experimental assessment of the absolute elevation limit of vascular plants. *Sci Rep*. 2016;6:24440. doi:10.1038/srep24440
40. Leipe C, Demske D, Tarasov PE, Wünnemann B, Riedel F. Potential of pollen and non-pollen palynomorph records from Tso Moriri (trans-Himalaya, NW India) for reconstructing Holocene limnology and human-environmental interactions. *Quat Int*. 2014;348:113-129. doi:10.1016/j.quaint.2014.02.026
41. Macek M, Dvorský M, Kopecký M, Wild J, Doležal J. Elevational range size patterns of vascular plants in the Himalaya contradict Rapoport's rule. *J Ecol*. 2021;109(12):4025-4037. doi:10.1111/1365-2745.13772
42. Ghosal S, Ahmed M. Pastoralism and Wetland Resources in Ladakh's Changthang Plateau. In: Prins HHT, Namgail T, eds. *Bird migration across the Himalayas: Wetland functioning amidst mountains and glaciers*. Cambridge University Press; 2017:333-341. doi:10.1017/9781316335420.025.
43. Baral HS, Bhandari BB. Importance of high altitude wetlands for protection of avian diversity in the Hindu Kush Himalayas. *The Initiation*. 2011;4:96-102. doi:10.3126/init.v4i0.5541
44. Prins HHT, van Wieren SE, Namgail T. Bird species diversity on a elevational gradient between the Greater Himalaya and the Tibetan plateau. In: Prins H, Namgail T, eds. *Bird migration across the Himalayas: Wetland functioning amidst mountains and glaciers*. Cambridge University Press; 2017:299-315.
45. Humbert-Droz B. Impacts of Tourism and Military Presence on Wetlands and Their Avifauna in the Himalayas. In: Prins HHT, Namgail T, eds. *Bird migration across the Himalayas: Wetland functioning amidst mountains and glaciers*. Cambridge University Press; 2017:342-358. doi:10.1017/9781316335420.026.
46. Goward S, Arvidson T, Williams D, Faundeen J, Irons J, Franks S. Historical record of Landsat global coverage: Mission operations, NSLRSDA, and international cooperator stations. *Photogrammetric Engineering and Remote Sensing*. 2006;72(10):1155-1169. doi:10.14358/PERS.72.10.1155
47. USGS. Historical international ground stations|Landsat missions. Published Online 2018. https://landsat.usgs.gov/historical-international-ground-stations/
48. Wulder MA, White JC, Loveland TR, et al. The global Landsat archive: status, consolidation, and direction. *Remote Sens Environ*. 2016;185:271-283. doi:10.1016/j.rse.2015.11.032
49. Guillevic P, Göttsche F, Nickeson J, et al. Land surface temperature product validation best practice protocol. Version 1.1. In: Guillevic P, Göttsche F, Nickeson J, Román M, eds. *Good practices for satellite-derived land product validation*; 2018. doi:10.5067/doc/ceoswgcv/lpv/lst.001.
50. Jin M, Dickinson RE. Land surface skin temperature climatology: benefitting from the strengths of satellite observations. *Environ Res Lett*. 2010;5(4):044004. doi:10.1088/1748-9326/5/4/044004
51. Mildrexler DJ, Zhao M, Running SW. A global comparison between station air temperatures and MODIS land surface temperatures reveals the cooling role of forests. *J Geophys Res Biogeo*. 2011;116(G3):1-15. doi:10.1029/2010JG001486
52. Duan SB, Li ZL, Li H, et al. Validation of collection 6 MODIS land surface temperature product using in situ measurements. *Remote Sens Environ*. 2019;225:16-29. doi:10.1016/j.rse.2019.02.020
53. Singh S, Bhardwaj A, Singh A, et al. Quantifying the congruence between air and land surface temperatures for various climatic and elevation zones of Western Himalaya. *Remote Sens (Basel)*. 2019;11(24):2889. doi:10.3390/rs11242889
54. Wang K, Wan Z, Wang P, Sparrow M, Liu J, Haginoya S. Evaluation and improvement of the MODIS land surface temperature/emissivity products using ground-based measurements at a semi-desert site on the western Tibetan plateau. *International Journal of Remote Sensing*. 2007;28(11):2549-2565. doi:10.1080/01431160600702665
55. Wang W, Liang S, Meyers T. Validating MODIS land surface temperature products using long-term nighttime ground measurements.

Remote Sens Environ. 2008;112(3):623-635. doi:10.1016/j.rse.2007.05.024
56. Hall DK, Riggs GA, Salomonson VV. Development of methods for mapping global snow cover using moderate resolution imaging spectroradiometer data. *Remote Sens Environ*. 1995;54(2):127-140. doi:10.1016/0034-4257(95)00137-P
57. R Core Team. R: a language and environment for statistical computing. R Foundation for statistical computing. 2022; https://www.R-project.org/
58. Gorelick N, Hancher M, Dixon M, Ilyushchenko S, Thau D, Moore R. Google earth engine: planetary-scale geospatial analysis for everyone. *Remote Sens Environ*. 2017;202:18-27. doi:10.1016/j.rse.2017.06.031
59. Liaw A, Wiener M. Classification and regression by randomForest. *R News*. 2002;2(3):18-22.
60. Wu Y, Duguay CR, Xu L. Assessment of machine learning classifiers for global lake ice cover mapping from MODIS TOA reflectance data. *Remote Sens Environ*. 2021;253:112206. doi:10.1016/j.rse.2020.112206
61. Dirscherl M, Dietz AJ, Kneisel C, Kuenzer C. Automated mapping of Antarctic Supraglacial Lakes using a machine learning approach. *Remote Sens (Basel)*. 2020;12(7):1203. doi:10.3390/rs12071203
62. Wendleder A, Schmitt A, Erbertseder T, D'Angelo P, Mayer C, Braun MH. Seasonal evolution of Supraglacial Lakes on Baltoro glacier from 2016 to 2020. *Front Earth Sci*. 2021;9:725394. doi:10.3389/feart.2021.725394
63. Berhane TM, Lane CR, Wu Q, et al. Decision-tree, rule-based, and random forest classification of high-resolution multispectral imagery for wetland mapping and inventory. *Remote Sens (Basel)*. 2018;10(4):580. doi:10.3390/rs1004058
64. Breiman L. Random forests. *Machine Learning*. 2001;45(1):5-32. doi:10.1023/A:1010933404324
65. Belgiu M, Drăgu L. Random forest in remote sensing: a review of applications and future directions. *ISPRS Journal of Photogrammetry and Remote Sensing*. 2016;114:24-31. doi:10.1016/j.isprsjprs.2016.01.011
66. Pal M. Random forest classifier for remote sensing classification. *International Journal of Remote Sensing*. 2005;26(1):217-222. doi:10.1080/01431160412331269698
67. Colditz RR. An evaluation of different training sample allocation schemes for discrete and continuous land cover classification using decision tree-based algorithms. *Remote Sens (Basel)*. 2015;7(8):9655-9681. doi:10.3390/rs70809655
68. Duguay CR, Bernier M, Gauthier Y, Kouraev A. Remote sensing of lake and river ice. In: Tedesco M, ed. *Remote sensing of the cryosphere*. John Wiley & Sons, Ltd; 2014:273-306. doi:10.1002/9781118368909.ch12.
69. Lauriol B, Clark J. Localisation, Genèse et Fonte de Quelques Naleds du Nord du Yukon (Canada). *Permafrost and Periglacial Processes*. 1991;2(3):225-236. doi:10.1002/ppp.3430020306
70. Bookhagen B. The influence of hydrology and glaciology on wetlands in the Himalayas. In: Prins HHT, Namgail T, eds. *Bird migration across the Himalayas: Wetland functioning amidst mountains and glacier*. Cambridge University Press; 2017:175-188. doi:10.1017/9781316335420.014.
71. Chatterjee A, Blom E, Gujja B, et al. WWF initiatives to study the impact of climate change on Himalayan high-altitude wetlands (HAWS). *Mountain Research and Development*. 2010;30(1):42-52. doi:10.1659/MRD-JOURNAL-D-09-00091.1
72. Lone SA, Jeelani G, Deshpande RD, Mukherjee A, Jasechko S, Lone A. Meltwaters dominate groundwater recharge in cold arid desert of upper Indus River Basin (UIRB), western Himalayas. *Sci Total Environ*. 2021;786:147514. doi:10.1016/j.scitotenv.2021.147514
73. Morse PD, Wolfe SA. Long-Term River icing dynamics in discontinuous permafrost, subarctic Canadian shield. *Permafrost and Periglacial Processes*. 2017;28(3):580-586. doi:10.1002/ppp.1907
74. Gagarin L, Wu Q, Melnikov A, et al. Morphometric analysis of groundwater icings: Intercomparison of estimation techniques. *Remote Sens (Basel)*. 2020;12(4):692. doi:10.3390/rs12040692

SUPPORTING INFORMATION

Additional supporting information can be found online in the Supporting Information section at the end of this article.

How to cite this article: Brombierstäudl D, Schmidt S, Nüsser M. Spatial and temporal dynamics of *aufeis* in the Tso Moriri basin, eastern Ladakh, India. *Permafrost and Periglac Process*. 2023;34(1):81-93. doi:10.1002/ppp.2173